

# Discovery of 146.8 s pulsations from EP J005146.9–730930, a new transient Be/X-ray binary in the SMC

F. Haberl<sup>1</sup>★, Y. Xu<sup>2</sup>†, C. Maitra<sup>1</sup>, G. Vasilopoulos<sup>3,4</sup>, W. Zhang<sup>5</sup>, W. Yuan<sup>5,6</sup>, C. Jin<sup>5,6,7</sup>, H.N. Yang<sup>5,1</sup>, L. Ducci<sup>8</sup>, D.M. Kaltenbrunner<sup>1</sup>, P. Maggi<sup>9</sup>, A. Rau<sup>1</sup>

<sup>1</sup>Max-Planck-Institut für extraterrestrische Physik, Gießenbachstraße 1, 85748 Garching, Germany

<sup>2</sup>Key Laboratory of Particle Astrophysics, Institute of High Energy Physics, Chinese Academy of Sciences, Beijing 100049, China

<sup>3</sup>Department of Physics, National and Kapodistrian University of Athens, University Campus Zografos, GR 15784, Athens, Greece

<sup>4</sup>Institute of Accelerating Systems & Applications, University Campus Zografos, Athens, Greece

<sup>5</sup>National Astronomical Observatories, Chinese Academy of Sciences, Beijing, 100101, People's Republic of China

<sup>6</sup>School of Astronomy and Space Sciences, University of Chinese Academy of Sciences, Beijing, 100049, People's Republic of China

<sup>7</sup>Institute for Frontier in Astronomy and Astrophysics, Beijing Normal University, Beijing, 102206, People's Republic of China

<sup>8</sup>Institut für Astronomie und Astrophysik, Sand 1, 72076 Tübingen, Germany

<sup>9</sup>Université de Strasbourg, CNRS, Observatoire astronomique de Strasbourg, UMR 7550, 67000 Strasbourg, France

Accepted 2025 July 22. Received 2025 July 22; in original form 2025 April 20

## ABSTRACT

Recent observations of the Small Magellanic Cloud (SMC) with *Einstein Probe* (*EP*) revealed a new transient X-ray source, most likely identified as Be/X-ray binary. To characterise the X-ray properties of EP J005146.9–730930 and in particular to look for pulsations in the X-ray flux, we triggered an *XMM-Newton* anticipated target of opportunity observation. To follow the flux evolution during the outburst we monitored the source for about three months with the Follow-up X-ray Telescope of *EP*. The *XMM-Newton* observation was performed on 2024 September 15 and we used the data from the European Photon Imaging Camera (EPIC) for detailed spectral and timing analyses. The EPIC X-ray spectrum is well described by an absorbed power law with photon index of  $1.25 \pm 0.04$  and the timing analysis revealed pulsations with  $146.79 \pm 0.03$  s. The source flux had decreased by a factor of about 10 since the observed maximum about one month before the *XMM-Newton* observation. EP J005146.9–730930 was never detected significantly during serendipitous observations before September 2024. The characteristics of the X-ray brightening suggest the source was discovered during a type II outburst reaching an X-ray peak luminosity of  $\sim 2 \times 10^{37}$  erg s<sup>-1</sup>. The trend of spectral hardening towards higher luminosities observed by *EP* suggests that the source is accreting below the critical luminosity, yielding an estimated lower limit for the pulsar magnetic field strength of  $3.3 \times 10^{12}$  G. The improved X-ray position confirms the candidate Be star OGLE J005147.58–730924.7 as optical counterpart. We conclude that EP J005146.9–730930 = SXP 146.8 is a new Be/X-ray binary pulsar in the SMC.

**Key words:** galaxies: individual (SMC) – X-rays: binaries – stars: emission-line, Be – stars: neutron pulsars: individual (EP J005146.9–730930)

## 1 INTRODUCTION

The Small Magellanic Cloud (SMC) is well known for the large population of high-mass X-ray binaries (HMXBs) with more than 125 systems known. About half of them revealed X-ray pulsations indicating the spin period of an accretion-powered neutron star. Since the compilation of the SMC HMXB catalogue by Haberl & Sturm (2016), seven new pulse periods from known or new Be/X-ray binaries (BeXRBs, the major subclass of HMXBs) were discovered (Vasilopoulos et al. 2016; Lazzarini et al. 2019; Vasilopoulos et al. 2020; Haberl et al. 2019; Kennea et al. 2020; Coe et al. 2023; Maitra et al. 2023), increasing the number of BeXRB pulsars to 70. The

large number of HMXBs is most likely related to the recent star formation history of the SMC which shows a maximum around 40 Myr ago. At this age the maximum occurrence of the Be phenomenon is expected (Antoniou et al. 2010).

BeXRBs are often discovered during X-ray outbursts. Periodic type-I outbursts (peak X-ray luminosities  $< 10^{37}$  erg s<sup>-1</sup>) occur around the periastron passage of the neutron star and tend to last only a small fraction of the binary period. Type-II outbursts are usually stronger ( $> 10^{37}$  erg s<sup>-1</sup>) and can last longer than the orbital period. For more details see the review by e.g. Reig (2011).

During recent monitoring observations of the SMC, a new transient source was discovered in data of the Follow-up X-ray Telescope (FXT) on board the newly launched *Einstein Probe* mission (*EP*; Yuan et al. 2022). The source, EP J005146.9–730930, was first detected by *EP-FXT* on 2024 July 25 at an 0.5–10 keV X-ray flux

★ E-mail: fwh@mpe.mpg.de

† E-mail: xuyj@ihep.ac.cn

of  $6.1 \times 10^{-13}$  erg cm $^{-2}$  s $^{-1}$ . EP J005146.9–730930 significantly brightened until August 2 ( $1.1 \times 10^{-11}$  erg cm $^{-2}$  s $^{-1}$ ) and August 15 ( $3.5 \times 10^{-11}$  erg cm $^{-2}$  s $^{-1}$ ). It remained near this flux level until August 29 ( $1.8 \times 10^{-11}$  erg cm $^{-2}$  s $^{-1}$ ) as reported by Xu et al. (2024). The flux increase was also seen during monitoring observations with the Neil Gehrels Swift observatory (Swift; Gehrels et al. 2004). EP J005146.9–730930 was detected in the data of the X-ray telescope (XRT) with a maximum count rate on August 13. From the improved X-ray position the candidate Be star OGLE J005147.58–730924.7 was proposed as optical counterpart (Kennea et al. 2024).

In order to look for pulsations we triggered one of our pre-approved anticipated target of opportunity observations with *XMM-Newton*. In Section 2 we describe the observations and the data analysis. The results are discussed in Section 3.

## 2 X-RAY OBSERVATIONS AND DATA ANALYSIS

### 2.1 Einstein Probe

The outburst of EP J005146.9–730930 was found by *EP* during a regular monitoring program of the SMC using FXT. *EP* observed EP J005146.9–730930 with multiple snapshots from 2024 July 25th to October 22nd (see Table 1 for details), then further observations of the corresponding SMC regions were prohibited due to solar constraints. *EP-FXT* consists of two identical and co-aligned telescope units, FXTA and FXTB, both observed EP J005146.9–730930 in the full-frame (FF) mode with thin filters.

We reduced the *EP-FXT* data following standard procedures using the FXT Data Analysis Software (FXTDAS) v1.10 with CALDB v1.10. The source spectra were extracted using a circular region with a radius of 50'' centered on the source position from FXTA and FXTB, respectively. Corresponding background spectra were selected from source-free areas with a radius of 300'' within the field-of-view. Due to the short exposure times of the individual *EP-FXT* monitoring observations, no periodicity was significantly detected in any of the single-epoch observations. Therefore, we only report the energy and flux evolution measured by *EP* in this paper. EP J005146.9–730930 and the nearby BeXRB SXP 172 (see below) could be resolved by FXT (on-axis half-power diameter spatial resolution of  $\lesssim 30''$ ) but not by the Wide-field X-ray Telescope (WXT) onboard *EP*. Therefore, in this paper we only report the X-ray fluxes measured by FXT. For spectral analysis, we group the energy spectra to have a minimum of one count in each bin, and jointly fit the FXTA and FXTB spectra in XSPEC (Arnaud 1996) using C-statistics (Cash 1979) to determine the best-fit parameters, which is preferable to  $\chi^2$ -statistics for low-count spectra.

#### 2.1.1 Spectral analysis

To study the spectral evolution of EP J005146.9–730930 during the outburst, we performed a spectral modeling of the multi-epoch observations taken by *EP-FXT*. We jointly fit the FXTA and FXTB spectra in the 0.2–10 keV band with an absorbed power-law model plus a cross-normalization constant: `constant*tbabs*tbvarabs*powerlaw`. The cross-normalization constant is allowed to vary freely for FXTB and is assumed to be unity for FXTA. For the absorption along the line of sight we used two components, one accounting for the foreground absorption in the Galaxy with abundances in the interstellar medium (ISM) following Wilms et al. (2000) and atomic cross-sections from Verner et al. (1996). The Galactic column density,  $N_{\text{H}}^{\text{Gal}}$ , was taken from

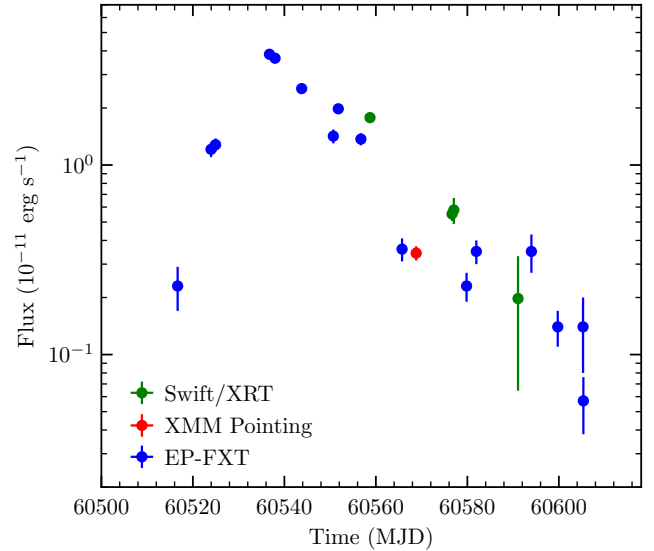


**Figure 1.** X-ray flux (observed, 0.2–10.0 keV) of EP J005146.9–730930 during the *EP-FXT* monitoring of the outburst. The flux derived from the *XMM-Newton* (Section 2.2.1) and *Swift* (Section 2.3) observations are included.

Dickey & Lockman (1990) and fixed in the fit at  $0.56 \times 10^{21}$  cm $^{-2}$ . For the absorption local to the source and in the ISM of the SMC, we assumed elemental abundances of 1.0 for He and 0.2 solar for elements with  $Z > 2$  (Russell & Dopita 1992) and left the column density free in the fit. The best-fit parameters measured during the *EP-FXT* monitoring observations, including the intrinsic absorption column density in the SMC,  $N_{\text{H}}^{\text{SMC}}$ , the power-law photon index,  $\Gamma$ , the X-ray flux in the 0.2–10 keV band, and the fitting statistics are listed in Table 1. As seen from the C-statistics, the model describes the FXT energy spectra well. The flux evolution during the X-ray outburst is plotted in Figure 1. The *EP-FXT* spectra together with the evolution of  $N_{\text{H}}^{\text{SMC}}$  and  $\Gamma$  as function of X-ray luminosity are shown in Figure 2. The *EP-FXT* observation on MJD 60565.7 was conducted about three days before the *XMM-Newton* observation. The best-fit parameters determined by *EP-FXT* on MJD 60565.7 could be considered as roughly consistent with the *XMM-Newton* results (see below) within errors, given that the *EP-FXT* parameters are less well constrained due to poorer statistics.

### 2.2 XMM-Newton

*XMM-Newton* carries three X-ray telescopes, two equipped with Metal Oxide Semi-conductor (MOS) CCD arrays (Turner et al. 2001) and one with a pn-CCD (Strüder et al. 2001). These detectors, which comprise the European Photon Imaging Camera (EPIC), are sensitive in the 0.15–12 keV energy band. The *XMM-Newton* observation was performed on 2024 September 15 (for details see Table 2).

We used the *XMM-Newton* Science Analysis Software (SAS) 21.0<sup>1</sup> package to process the EPIC data. To exclude time intervals of high background during soft-proton flares, we filtered out time intervals with background rates in the 7.0–15.0 keV band above 8 and 2.5 cts ks $^{-1}$  arcmin $^{-2}$  for EPIC-pn and EPIC-MOS, respectively. The X-ray position of EP J005146.9–730930 was determined using the standard *XMM-Newton* source detection task `edetect_chain` on the

<sup>1</sup> <https://www.cosmos.esa.int/web/xmm-newton/sas>

**Table 1.** *EP*-FXT monitoring observations of EPJ005146.9–730930 with the best-fit spectral parameters. Both FXTA and FXTB data were taken in the FF mode, pile-up effects were negligible at such flux levels (Zhang et al. 2025). The best-fit spectral parameters of  $N_{\text{H}}^{\text{SMC}}$  and  $\Gamma$  are obtained from joint fits of FXTA and FXTB. The net count rates and the observed X-ray flux in the 0.2–10 keV band listed are the average values obtained by FXTA and FXTB. All uncertainties quoted are at the 90% confidence level.

No.	ObsID	Observation time (UT)	Exposure (s)	Net count rate ( $10^{-2} \text{ s}^{-1}$ )	$N_{\text{H}}^{\text{SMC}}$ ( $10^{21} \text{ cm}^{-2}$ )	$\Gamma$	Flux <sub>0.2–10 keV</sub> ( $\text{erg cm}^{-2} \text{ s}^{-1}$ )	Cstat/dof
1	11908398338	2024-07-25 15:59 – 07-25 16:18	1148	$3.0 \pm 0.4$	$<9.7$	$0.7^{+0.6}_{-0.3}$	$(2.3 \pm 0.6) \times 10^{-12}$	70.9/61
2	11908398339	2024-08-01 23:05 – 08-01 23:23	1075	$20.6 \pm 1.0$	$13 \pm 5$	$1.1 \pm 0.2$	$(1.21 \pm 0.11) \times 10^{-11}$	271.0/328
3	11908428547	2024-08-02 23:08 – 08-02 23:29	1288	$23.1 \pm 0.9$	$9.8^{+4.3}_{-3.8}$	$1.0 \pm 0.2$	$(1.28 \pm 0.10) \times 10^{-11}$	312.0/412
4	11908398374	2024-08-14 17:24 – 08-14 17:56	979	$55.5 \pm 1.7$	$2.3^{+1.7}_{-1.5}$	$0.7 \pm 0.1$	$(3.84 \pm 0.21) \times 10^{-11}$	486.5/595
5	11908428567	2024-08-15 22:56 – 08-15 23:19	1405	$63.5 \pm 1.5$	$3.1^{+1.3}_{-1.5}$	$0.8 \pm 0.1$	$(3.66 \pm 0.15) \times 10^{-11}$	699.4/767
6	11908525313	2024-08-21 18:27 – 08-21 18:53	1545	$39.9 \pm 1.1$	$3.9^{+1.9}_{-1.7}$	$0.9 \pm 0.1$	$(2.53 \pm 0.13) \times 10^{-11}$	565.2/617
7	11908553988	2024-08-28 16:41 – 08-28 16:57	969	$25.0 \pm 1.1$	$6.7^{+3.7}_{-2.2}$	$1.0 \pm 0.2$	$(1.42 \pm 0.12) \times 10^{-11}$	284.5/340
8	11908561156	2024-08-29 18:49 – 08-29 19:12	1306	$33.9 \pm 1.1$	$3.5^{+2.5}_{-2.1}$	$0.8 \pm 0.1$	$(1.98 \pm 0.12) \times 10^{-11}$	456.1/529
9	11908572422	2024-09-03 17:19 – 09-03 17:47	1648	$21.3 \pm 0.8$	$4.9^{+3.0}_{-2.7}$	$0.9 \pm 0.2$	$(1.37 \pm 0.10) \times 10^{-11}$	355.2/451
10	11908609289	2024-09-12 17:23 – 09-12 17:44	1275	$10.6 \pm 0.6$	$15^{+9}_{-7}$	$1.6^{+0.4}_{-0.3}$	$(3.6 \pm 0.5) \times 10^{-12}$	164.3/222
11	11908656897	2024-09-26 19:49 – 09-26 20:09	1224	$6.8 \pm 0.5$	$15^{+10}_{-8}$	$1.6 \pm 0.5$	$(2.3 \pm 0.4) \times 10^{-12}$	136.9/143
12	11908663553	2024-09-28 22:45 – 09-28 23:27	1571	$6.3 \pm 0.5$	$<9.3$	$1.0^{+0.4}_{-0.3}$	$(3.5 \pm 0.5) \times 10^{-12}$	137.8/170
13	11908712722	2024-09-26 19:49 – 09-26 20:09	867	$4.4 \pm 0.5$	$<8.5$	$0.7^{+0.6}_{-0.3}$	$(3.5 \pm 0.8) \times 10^{-12}$	57.6/68
14	11908731657	2024-10-16 18:05 – 10-16 18:30	1459	$2.7 \pm 0.3$	$<15.1$	$1.0^{+0.6}_{-0.5}$	$(1.4 \pm 0.3) \times 10^{-12}$	77.9/73
15	11908753155	2024-10-10 23:55 – 10-11 00:09	1104	$1.7 \pm 0.3$	$<11.5$	$0.6^{+0.7}_{-0.5}$	$(1.4 \pm 0.6) \times 10^{-12}$	40.3/32
16	11908754179	2024-10-22 08:23 – 10-22 08:39	971	$2.3 \pm 0.4$	$<13.9$	$1.7^{+1.2}_{-0.5}$	$(5.7 \pm 1.9) \times 10^{-13}$	23.2/38

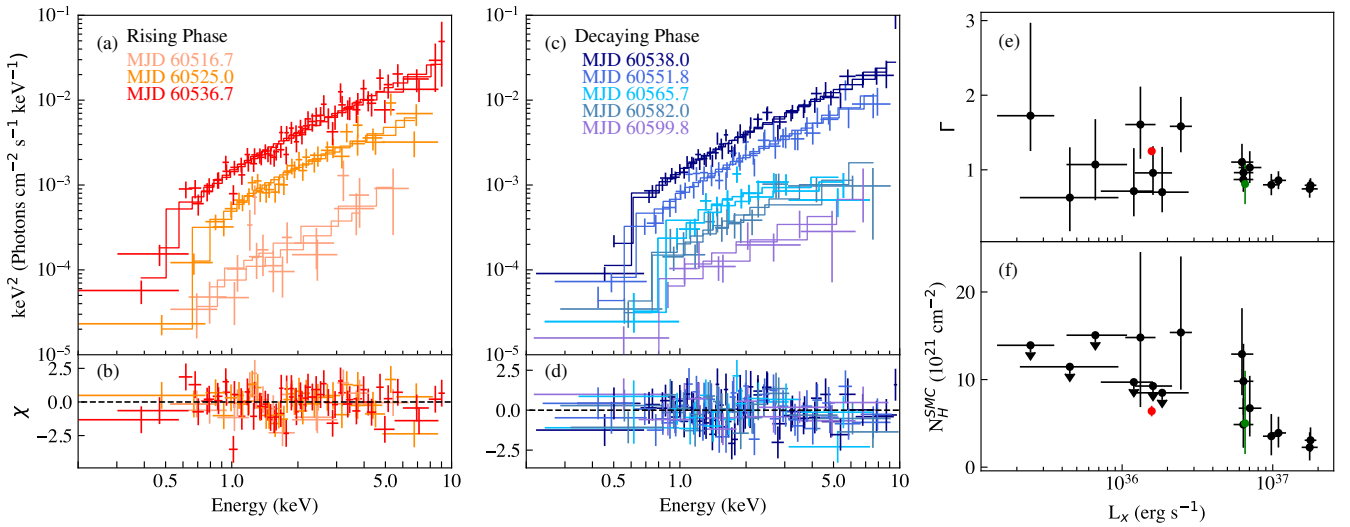


**Figure 2.** Left: *EP*-FXT energy spectra folded with the best-fit models during the rising phase of the outburst (a), along with the spectral residuals (b). FXTA and FXTB spectra taken in a single epoch are plotted in the same color, and are rebinned for visual clarity. Middle: Sample *EP*-FXT spectra during the decaying phase of the outburst. Right: Relation of the photon index (e) and the intrinsic absorption column density in SMC along the line-of-sight of EPJ005146.9–730930 (f) with the absorption-corrected X-ray luminosity in 0.2–10 keV, assuming a source distance of 62 kpc. Measurements by *EP*, *XMM-Newton*, and *Swift* are plotted in black, red, and green, respectively.

**Table 2.** The *XMM-Newton* observation of EPJ005146.9–730930. The net exposure times used for the EPIC spectra and images after background-flare screening are listed for pn, MOS1 and MOS2, respectively.

Instrument	Observation ID	Observation time (UT)	Net exposure time	
			(ks)	Fraction of total
EPIC	0903450101	2024-09-15 16:19 – 22:46	9.00, 13.25, 13.22	67%, 77%, 76%

**Table 3.** Astrometric alignments.

X-ray source	R.A. (J2000) Dec. EPIC uncorrected		$1\sigma$ Err (")	R.A. (J2000) Dec. Gaia DR3		R.A. (J2000) Dec. EPIC corrected		$1\sigma$ Err (")
	(h m s)	( $^{\circ}$ ' ")		(h m s)	( $^{\circ}$ ' ")	(h m s)	( $^{\circ}$ ' ")	
EP J005146.9–730930	00 51 47.695	-73 09 25.60	0.51	00 51 47.584	-73 09 25.15	00 51 47.59	-73 09 25.1	0.1
SXP 172	00 51 52.126	-73 10 34.66	0.50	00 51 52.025	-73 10 34.14	00 51 52.03	-73 10 34.1	0.1

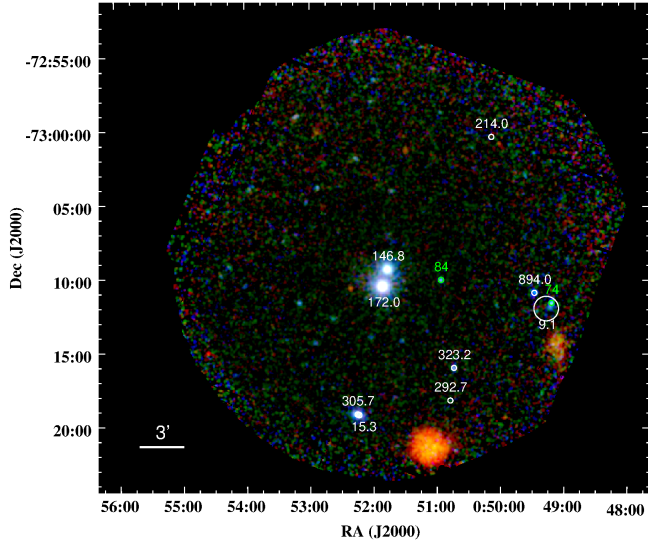


**Figure 3.** *XMM-Newton* EPIC colour image. Red, green and blue represent the detector-background-subtracted and vignetting-corrected count rate images in the bands 0.2–1.0 keV, 1.0–2.0 keV and 2.0–4.5 keV, respectively. HMXBs from Haberl & Sturm (2016) known in the field are marked with their pulse period (white), if known, or catalogue numbers otherwise. An association of the 9.1 s pulsar with source 74 still needs confirmation.

EPIC images after screening for the background flaring. The uncertainty is dominated by the remaining systematic error of  $0.5''$ . The position is  $1.1''$  from OGLE J005147.58–730924.7, the optical counterpart proposed by Kennea et al. (2024) and  $0.63''$  from the Gaia DR3 position (Gaia Collaboration 2022) of the counterpart. During the *XMM-Newton* observation the nearby BeXRB SXP 172 ( $\sim 70''$  angular distance; Laycock et al. 2010; Antoniou et al. 2009) was a factor of  $\sim 2.5$  brighter than EP J005146.9–730930 (see Figure 3). Its derived X-ray position is also shifted by about the same amount and direction with respect to the Gaia DR3 position of its identified counterpart (see Table 3). Due to the small angular distance between the two sources field distortions and rotation can be neglected. Therefore, we used SXP 172 to compute a linear astrometric correction of  $-0.44''$  and  $+0.52''$  in R.A. and Dec. for the X-ray position of EP J005146.9–730930. The resulting final X-ray coordinates for EP J005146.9–730930 are presented in Table 3, fully consistent with the Gaia position within  $0.1''$ .

For the extraction of EPIC spectra and light curves we defined circular regions with radii of  $30''$  and  $60''$  for the source and a nearby source-free background region, respectively. The EPIC spectra were grouped to a minimum of 20 counts per bin. For the timing analysis of the EPIC-pn data we used the first 11 ks of the observation, which includes some weak flares but excludes the very strong background flares during the last part of the observation. The source shows little flux variations during the observation.

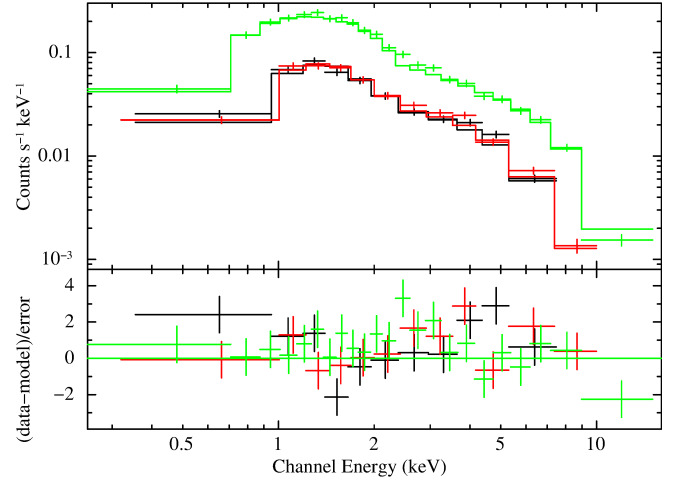


**Figure 4.** Top: *XMM-Newton* EPIC spectra of EP J005146.9–730930 with best-fit model as histograms (MOS1: black, MOS2: red, pn: green). Bottom: Residuals in error units.

### 2.2.1 EPIC spectral analysis

The X-ray spectrum of EP J005146.9–730930 during the *XMM-Newton* observation was analysed by simultaneously fitting the model from above to the three EPIC spectra. Again, a cross-normalization constant was included which was fixed at 1.0 for the MOS1 spectrum and allowed to vary freely for the other two spectra. This model describes the spectra well with a  $\chi^2$  of 469.0 for 440 degrees of freedom. The EPIC spectra with their best-fit model are presented in Figure 4 and the best-fit model parameters are summarised in Table 4. The observed flux (0.2–10.0 keV, averaged over the three instruments) was  $3.43 \times 10^{-12}$  erg cm $^{-2}$  s $^{-1}$  which can be converted to an absorption corrected luminosity of  $1.85 \times 10^{36}$  erg s $^{-1}$ , assuming a distance of 62 kpc to the SMC (Graczyk et al. 2020).

### 2.2.2 EPIC-pn timing analysis

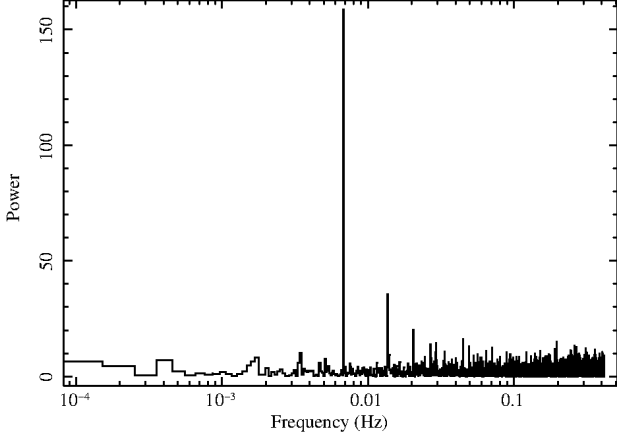
To investigate short-term variability of EP J005146.9–730930, we created EPIC-pn light curves in the 0.2–8.0 keV energy band from the source extraction region. We selected valid pixel patterns (PATTERN 1–12) and corrected the event arrival times to the solar system barycentre. For our search for X-ray pulsations in the light curves, we first created power spectra which revealed pulsations at a frequency of about 6.8 mHz. The power spectrum obtained from the 0.2–8.0 keV EPIC-pn light curve is presented in Figure 5. Besides the fundamental frequency, also the first harmonic at about 13.6 mHz is visible.

Following recent work on other HMXB pulsars in the Magellanic Clouds (e.g. Haberl et al. 2022; Vasilopoulos et al. 2017), we determined the precise period and its error in a second step. For this we used the Bayesian approach described by Gregory & Loredo (1996)

**Table 4.** *XMM-Newton* and *Swift* spectral analysis results of EP J005146.9–730930. Errors on spectral fit parameters are given for 90% confidence intervals.

Instrument	$N_{\text{H}}^{\text{Gal}}$ ( $10^{21} \text{ cm}^{-2}$ )	$N_{\text{H}}^{\text{SMC}}$ ( $10^{21} \text{ cm}^{-2}$ )	Photon index	$F_{\text{x}}^a$ ( $\text{erg cm}^{-2} \text{ s}^{-1}$ )	$L_{\text{x}}^a$ ( $\text{erg s}^{-1}$ )	$\chi_r^2/\text{dof}$
<i>XMM-Newton</i> EPIC	0.56 fixed	$6.4 \pm 0.6$	$1.25 \pm 0.04$	$3.43 \times 10^{-12}$	$1.85 \times 10^{36}$	1.07/440
<i>Swift</i> -XRT	0.56 fixed	$5.0^{+6.0}_{-3.5}$	$0.81 \pm 0.27$	$1.43 \times 10^{-11}$	$7.03 \times 10^{36}$	0.54/14

<sup>a</sup>Observed X-ray flux and absorption-corrected luminosity in the 0.2–10 keV band assuming a distance of 62 kpc.

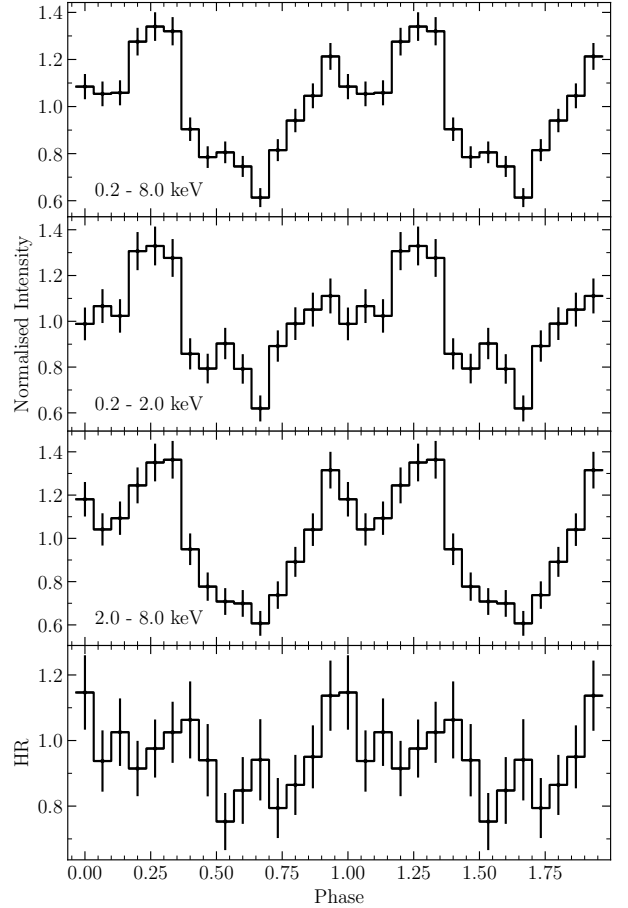

**Figure 5.** Power spectrum of EP J005146.9–730930 derived from the 0.2–8.0 keV EPIC-pn light curve with 1.2 s binning.

in a restricted frequency range around the peak detected in the power spectrum. This results in a pulse period of  $146.79 \pm 0.03$  s.

The pulse profiles in different energy bands, together with the corresponding hardness ratio (HR), are shown in Figure 6. As already indicated by the presence of the first harmonic in the power spectrum, the pulse profile is double-peaked. The earlier of the two peaks is more pronounced at energies above 2 keV, which leads to a maximum in the HR, while lower HRs are indicated during the intensity minimum. We infer a pulsed fraction of  $36 \pm 8\%$  ( $0.5 \times (\text{maximum} - \text{minimum}) / \text{mean}$ ) from the broad (0.2–8.0 keV) band. We computed the pulsed fraction as a function of energy following (Ferrigno et al. 2023). In particular, we used the FFT, RMS, and area methods and computed the pulsed fraction for nine energy ranges between 0.2 and 8.0 keV, with the results shown in Figure 7. The results reveal somewhat smaller pulsed fraction values below 1 keV, but no significant features are identified, in contrast to other bright outbursts in the Magellanic Clouds (Yang et al. 2025).

### 2.3 Long-term X-ray behaviour

We used the High-energy Light curve GeneraTor (HILIGT; König et al. 2022; Saxton et al. 2022)<sup>2</sup> to investigate the long-term X-ray light curve of EP J005146.9–730930. The tool uses available catalogues to search for source detections and provides upper limits ( $2\sigma$ ) when the source was not detected. We excluded *ROSAT* data because of the limited energy band and spatial resolution. We mainly obtained upper limits from archival observations performed with *Swift* and *XMM-Newton* before September 2024. To determine the conversion factor for *Swift*-XRT count rates (0.2–12 keV) to fluxes (0.2–10 keV) we downloaded the spectrum obtained on 2024-09-05 16:12–18:08 UT (ObsID 00016793001, exposure 2.50 ks), when


**Figure 6.** Pulse profiles, normalised to the average count rates, obtained from folding the EPIC-pn light curves in broad, soft and hard energy bands (top three panels). The hardness ratio (HR, bottom) was derived as count ratio of hard to soft bands.

the flux measured by *Swift* was highest, from the *Swift* archive<sup>3</sup> (Evans et al. 2009) and modelled it consistently to the EPIC spectra. The best-fit model parameters are listed in Table 4. This resulted in a conversion factor of  $1.02 \times 10^{-10} \text{ erg cm}^{-2} \text{ s}^{-1} / (\text{cts s}^{-1})$ . For *XMM-Newton* we used the fluxes provided by HILIGT (assuming a power law with photon index 1.5 and an absorption column density of  $10^{21} \text{ cm}^{-2}$ ). To convert the HILIGT 0.2–12 keV fluxes to 0.2–10.0 keV band we simulated an EPIC-pn spectrum with the HILIGT model parameters and normalised it to the count rate obtained from the observed spectrum.

Because EP J005146.9–730930 was not detected by eROSITA (Predehl et al. 2021), we determined upper limits from the four

<sup>2</sup> <http://xmmuls.esac.esa.int/upperlimitserver/>

<sup>3</sup> [https://www.swift.ac.uk/user\\_objects/index.php](https://www.swift.ac.uk/user_objects/index.php)

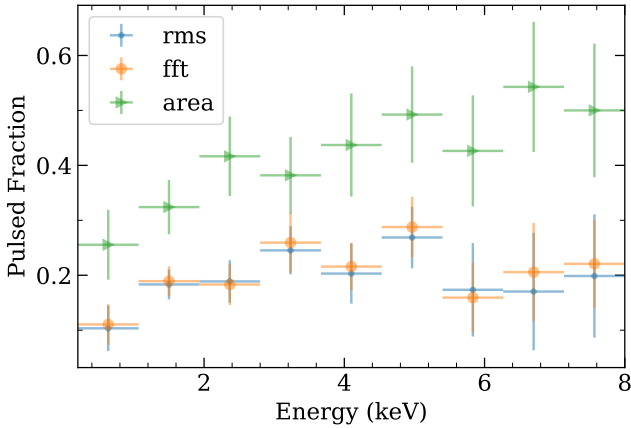


**Figure 7.** Pulse profile as a function of energy. The pulsed fraction is computed using three methods outlined in Ferrigno et al. (2023).

eROSITA surveys, which covered the source. Due to the vicinity of SXP 172 and the size of the point spread function of  $\sim 30''$  (half energy width in survey mode, Merloni et al. 2024) SXP 172 contributes to the flux at the position of EP J005146.9–730930. Therefore, we extracted source and background spectra, with the background region at the same distance to SXP 172, but on the opposite side of EP J005146.9–730930 in order to take the contribution from this brighter source into account. Assuming the best-fit spectral model from the EPIC spectra, normalised to the  $2\sigma$  count rate upper limits inferred from the spectra, we computed fluxes in the 0.2–10.0 keV band. Finally, the 0.2–10.0 keV fluxes measured by EP and from the new *XMM-Newton* observation were included in the light curve, which is plotted in Figure 8 (see also Figure 1). It reveals the first strong X-ray outburst seen from EP J005146.9–730930 with a maximum flux a factor of at least 2340 higher than the most stringent upper limit inferred from an *XMM-Newton* observation in 2009.

### 3 DISCUSSION

After the discovery of a new X-ray transient in the SMC by EP, we observed EP J005146.9–730930 with *XMM-Newton* during its outburst. The *XMM-Newton* observation was performed 31 days after the maximum source flux was observed by EP, when the flux had declined by a factor of  $\sim 10$ . The EPIC data reveal a highly significant coherent signal at a period of  $146.79 \pm 0.03$  s, which is close to the maximum of the second peak in the pulse-period distribution of BeXRB pulsars in the SMC (Haberl & Sturm 2016). The light curve folded at the pulse period shows a double-peaked profile with pulsed fraction of 36 %, also typical for BeXRBs.

Based on the EP-FXT monitoring light curve (see Figure 1), the outburst of EP J005146.9–730930 followed a fast-rise-slow-decay profile, lasting more than 90 days. From the EP-FXT spectral analysis results, the absorption corrected X-ray flux in the 0.2–10 keV band reached at least,  $L_{\text{peak}} \sim 1.8 \times 10^{37}$  erg s $^{-1}$ , near the peak of the outburst ( $L_{\text{peak}}/L_{\text{Edd}} \sim 0.1$ , here the Eddington luminosity for a neutron star is taken as  $1.7 \times 10^{38}$  erg s $^{-1}$ ), indicating that EP J005146.9–730930 likely went into a type-II outburst of a transient BeXRB despite the peak luminosity being at the lower end of the distributions of typical values (Reig 2011). EP-FXT observed EP J005146.9–730930 in outburst covering the change over nearly

two orders of magnitude in luminosity, enabling us to investigate the relation of its spectral properties with luminosity.

The spectral evolution of BeXRBs during type-II outbursts has been more thoroughly studied for Galactic sources (e.g., Reig 2008; Tamang et al. 2022; Thalhammer et al. 2024). The spectral behaviour of EP J005146.9–730930 is consistent with the typical cases known for Galactic sources accreting at relatively low Eddington ratios, in the sense that the energy spectra hardened when the source luminosity became higher (see Figure 2e). Considering the most tightly constrained data points, we find that the photon index measured by EP-FXT,  $\Gamma \sim 0.7$ – $0.8$ , around the peak of the outburst is significantly smaller than that obtained based on *XMM-Newton*,  $\Gamma = 1.25 \pm 0.04$ . The decrease of photon index and the increase of absorption column density could both cause spectral hardening. The hardness-intensity diagram of EP J005146.9–730930 during outburst measured by EP in Figure 9a displays a similar trend as Figure 2e, indicating that the spectral hardening behaviour towards high luminosities is model-independent. Also, we plot the confidence contours in Figure 9b to investigate the level of parameter degeneracy between  $N_{\text{H}}^{\text{SMC}}$ , and  $\Gamma$ . As an example, the best fit of the EP data on MJD 60538.0 prefers both lower  $N_{\text{H}}^{\text{SMC}}$  and smaller  $\Gamma$  when compared to that on MJD 60565.7 above  $3\sigma$  confidence, with a difference of about ten times in luminosity.

The spectral evolution of EP J005146.9–730930 supports the general picture of an accreting neutron star below a certain critical luminosity that is largely determined by the pulsar magnetic field, when the deceleration of the accreting flow at the vicinity of the neutron star surface is dominated by Coulomb interactions rather than radiation pressure (Basko & Sunyaev 1976). Under such circumstances, the increase in luminosity is believed to lead to a decrease in the height of the emission zone in the accretion column above the neutron star surface, hence larger optical depth for the Comptonisation process and producing harder photons (Becker et al. 2012; Reig & Nespoli 2013). For an approximate estimate, assuming the critical luminosity,  $L_{\text{crit}} > L_{\text{peak}}$ , and a relation of the critical luminosity with the neutron star surface magnetic field<sup>4</sup>, we could obtain a lower limit for the magnetic field of EP J005146.9–730930 as,  $B > 3.3 \times 10^{12}$  G.

There are also hints for a tentative anti-correlation between the absorption column density and the source luminosity (see Figure 2f), which could be caused by absorption variations related to orbital geometrical effects, similar as observed during a recent giant outburst of the Galactic BeXRB EXO 2030+375 (Thalhammer et al. 2024). We note that the measurements of  $N_{\text{H}}^{\text{SMC}}$  derived from EP J005146.9–730930 are subject to large uncertainties, as only upper limits are yielded by the last few EP observations. Based on only the data points with constrained measurements from EP, *XMM-Newton*, and *Swift*, the standard Pearson correlation coefficient between the absorption column density,  $N_{\text{H}}^{\text{SMC}}$ , and the logarithmic X-ray luminosity,  $L_x$ , is found to be  $-0.746$ , with a  $p$ -value of 0.005, indicating an anti-correlation with a confidence of  $\sim 2.79\sigma$ .

During many serendipitous X-ray observations before 2024 EP J005146.9–730930 was never significantly detected. Many short observations yielded relatively non-constraining  $2\sigma$  upper limits. Formally, only one measurement was indicated as detection, but the flux is again only twice its error. Two *XMM-Newton* pointed observations provide stringent upper limits about three orders of magnitude

<sup>4</sup> The critical luminosity is derived to be  $1.5 \times 10^{37} B_{12}^{16/15}$  erg s $^{-1}$  in Becker et al. (2012). And here we multiply the absorption-corrected luminosity in the 0.2–10 keV band by a factor of 3 to estimate the bolometric luminosity of EP J005146.9–730930.

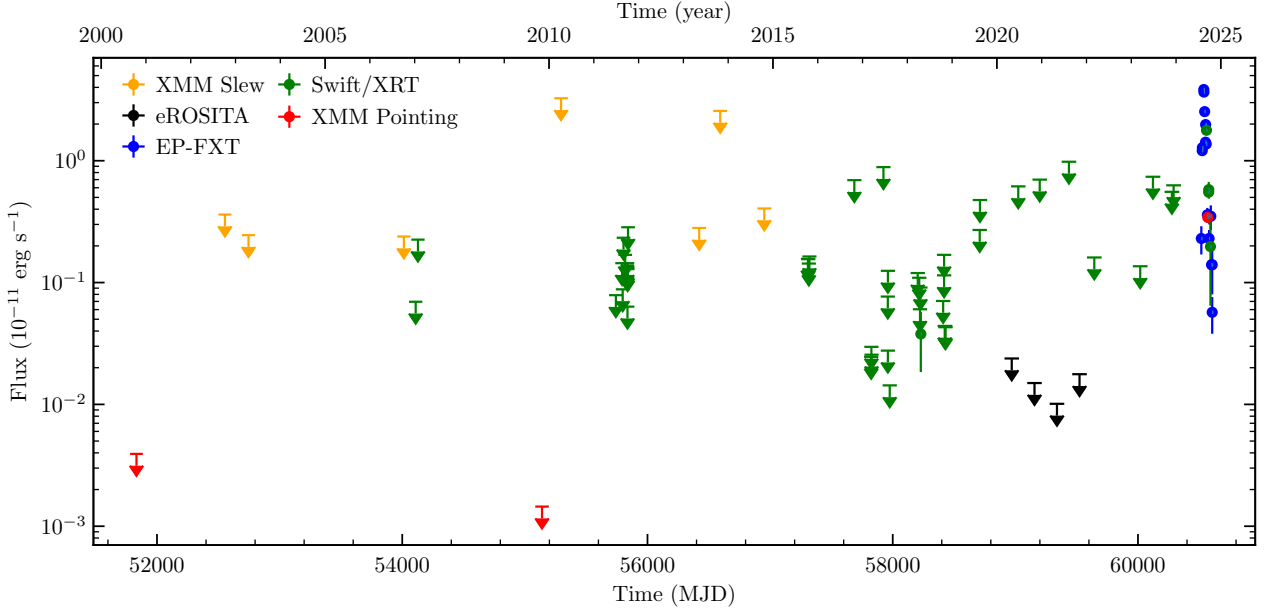


**Figure 8.** Long-term X-ray flux (observed, 0.2–10.0 keV) evolution of EP J005146.9–730930. Down-arrows mark  $2\sigma$  upper limits. The evolution of the X-ray outburst with expanded time axis is shown in Figure 1.

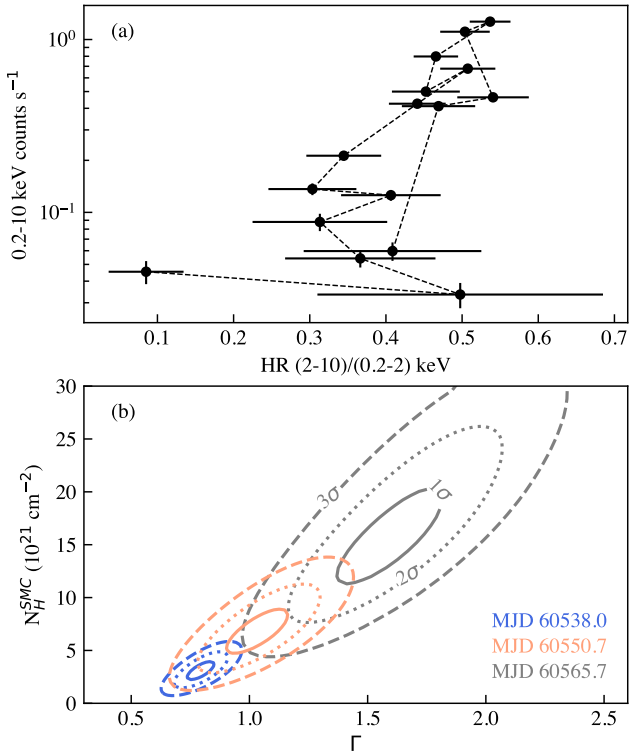


**Figure 9.** The hardness-intensity diagram measured by *EP* during the outburst of EP J005146.9–730930 (a). The hardness ratio is defined as the ratio of the count rates in the energy band of 2–10 keV and 0.2–2 keV. The quoted numbers are the average measurements by FXTA and FXTB. Confidence contours of the absorption column density,  $N_{\text{H}}^{\text{SMC}}$ , and the photon index,  $\Gamma$  determined from three representative *EP* observations on MJD 60538.0, 60550.7, and 60565.7 (b).

below the maximum observed during outburst. Duration, high amplitude and maximum X-ray luminosity of  $\sim 2 \times 10^{37}$  erg  $\text{s}^{-1}$  all suggest that EP J005146.9–730930 was for the first time detected in X-rays during a type-II outburst.

#### ACKNOWLEDGEMENTS

This work is based on data obtained with *Einstein Probe* and *XMM-Newton*. *Einstein Probe* is a space mission supported by the Strategic Priority Program on Space Science of Chinese Academy of Sciences, in collaboration with ESA, MPE and CNES (grant no. XDA15310000), the Strategic Priority Research Program of the Chinese Academy of Sciences (grant no. XDB0550200), and the National Key R&D Program of China (2022YFF0711500). Y.X. acknowledges support by the Hundred Talents Program of the Chinese Academy of Sciences. C.J. acknowledges the National Natural Science Foundation of China through grant 12473016. LD acknowledges funding from German Research Foundation (DFG), Projektnummer 549824807. *XMM-Newton* is an ESA science mission with instruments and contributions directly funded by ESA Member States and NASA. The *XMM-Newton* project is supported by the DLR and the Max Planck Society. This work made use of data supplied by the UK Swift Science Data Centre at the University of Leicester.

#### DATA AVAILABILITY

The data presented in the tables and figures of the paper are available upon reasonable request from the corresponding author. The data from the *XMM-Newton* observation will become available from the *XMM-Newton* Science Archive<sup>5</sup> at the end of September 2025.

<sup>5</sup> <https://www.cosmos.esa.int/web/xmm-newton/xsa>

## REFERENCES

- Antoniou V., Hatzidimitriou D., Zezas A., Reig P., 2009, *ApJ*, 707, 1080
- Antoniou V., Zezas A., Hatzidimitriou D., Kalogera V., 2010, *ApJ*, 716, L140
- Arnaud K. A., 1996, in ASP Conf. Ser. 101: Astronomical Data Analysis Software and Systems V. p. 17
- Basko M. M., Sunyaev R. A., 1976, *MNRAS*, 175, 395
- Becker P. A., et al., 2012, *A&A*, 544, A123
- Cash W., 1979, *ApJ*, 228, 939
- Coe M. J., Kennea J. A., Gaudin T. M., Monageng I., Townsend L., Buckley D. A., Udalski A., Evans P., 2023, The Astronomer’s Telegram, 16321, 1
- Dickey J. M., Lockman F. J., 1990, *ARA&A*, 28, 215
- Evans P. A., et al., 2009, *MNRAS*, 397, 1177
- Ferrigno C., D’Ài A., Ambrosi E., 2023, *A&A*, 677, A103
- Gaia Collaboration 2022, VizieR Online Data Catalog: Gaia DR3 Part 1. Main source (Gaia Collaboration, 2022), VizieR On-line Data Catalog: I/355. Originally published in: Astron. Astrophys., in prep. (2022), doi:10.26093/cds/vizie.1355
- Gehrels N., et al., 2004, *ApJ*, 611, 1005
- Graczyk D., et al., 2020, *ApJ*, 904, 13
- Gregory P. C., Lored T. J., 1996, *ApJ*, 473, 1059
- Haberl F., Sturm R., 2016, *A&A*, 586, A81
- Haberl F., et al., 2019, The Astronomer’s Telegram, 13312, 1
- Haberl F., Maitra C., Vasilopoulos G., Maggi P., Udalski A., Monageng I. M., Buckley D. A. H., 2022, *A&A*, 662, A22
- Kennea J. A., Coe M. J., Evans P. A., Monageng I. M., Townsend L. J., Siegel M. H., Udalski A., Buckley D. A. H., 2020, The Astronomer’s Telegram, 13823, 1
- Kennea J. A., Gaudin T. M., Evans P. A., Coe M. J., 2024, The Astronomer’s Telegram, 16796, 1
- König O., et al., 2022, *Astronomy and Computing*, 38, 100529
- Laycock S., Zezas A., Hong J., Drake J. J., Antoniou V., 2010, *ApJ*, 716, 1217
- Lazzarini M., et al., 2019, *ApJ*, 884, 2
- Maitra C., Haberl F., Kaltenbrunner D., Doroshenko V., Ducci L., Udalski A., 2023, The Astronomer’s Telegram, 15886, 1
- Merloni A., et al., 2024, *A&A*, 682, A34
- Predehl P., et al., 2021, *A&A*, 647, A1
- Reig P., 2008, *A&A*, 489, 725
- Reig P., 2011, *Ap&SS*, 332, 1
- Reig P., Nespoli E., 2013, *A&A*, 551, A1
- Russell S. C., Dopita M. A., 1992, *ApJ*, 384, 508
- Saxton R. D., et al., 2022, *Astronomy and Computing*, 38, 100531
- Strüder L., et al., 2001, *A&A*, 365, L18
- Tamang R., Ghising M., Tobrej M., Rai B., Paul B. C., 2022, *MNRAS*, 515, 5407
- Thalhammer P., et al., 2024, *A&A*, 688, A213
- Turner M. J. L., et al., 2001, *A&A*, 365, L27
- Vasilopoulos G., Haberl F., Antoniou V., Zezas A., 2016, The Astronomer’s Telegram, 9229, 1
- Vasilopoulos G., Zezas A., Antoniou V., Haberl F., 2017, *MNRAS*, 470, 4354
- Vasilopoulos G., et al., 2020, *MNRAS*, 494, 5350
- Verner D. A., Ferland G. J., Korista K. T., Yakovlev D. G., 1996, *ApJ*, 465, 487
- Wilms J., Allen A., McCray R., 2000, *ApJ*, 542, 914
- Xu Y. J., et al., 2024, The Astronomer’s Telegram, 16795, 1
- Yang H. N., et al., 2025, *MNRAS*, 536, 1357
- Yuan W., Zhang C., Chen Y., Ling Z., 2022, in Bambi C., Sanganelo A., eds, , Handbook of X-ray and Gamma-ray Astrophysics. p. 86, doi:10.1007/978-981-16-4544-0\_151-1
- Zhang J., et al., 2025, *Radiat. Detect. Technol. Methods*

This paper has been typeset from a  $\text{\TeX}/\text{\LaTeX}$  file prepared by the author.